

# Deglacial Pulse of Neutralized Carbon from the Pacific Seafloor: A Natural Analog for Ocean Alkalinity Enhancement?

Ryan Andrew Green<sup>1</sup>, Mathis P Hain<sup>1</sup>, and Patrick A Rafter<sup>2</sup>

<sup>1</sup>University of California, Santa Cruz

<sup>2</sup>University of California, Irvine

January 15, 2024

1 **Deglacial Pulse of Neutralized Carbon from the Pacific Seafloor: A Natural Analog for**  
2 **Ocean Alkalinity Enhancement?**

3 **R. A. Green<sup>1</sup>, M. P. Hain<sup>1</sup>, and P. A. Rafter<sup>2</sup>**

4 <sup>1</sup> Earth and Planetary Science Department, University of Santa Cruz, Santa Cruz, USA

5 <sup>2</sup> College of Marine Science, University of South Florida, St. Petersburg, FL, USA

6

7 Corresponding author: Ryan A. Green (rygreen@ucsc.edu)

8 **Key Points:**

- 9 • Observed deglacial changes in atmospheric CO<sub>2</sub> and <sup>14</sup>C/C allow for up to 2397 Pg of  
10 neutralized geologic carbon (i.e., bicarbonate) release
- 11 • The global carbon cycle is essentially “blind” to neutralized carbon release, only  
12 constrained by <sup>14</sup>C budget
- 13 • This gigaton-scale neutralized carbon release may be a natural analog to the marine CO<sub>2</sub>  
14 removal method of ocean alkalinity enhancement
- 15

## 16 **Abstract**

17 The ocean carbon reservoir controls atmospheric carbon dioxide (CO<sub>2</sub>) on millennial timescales.  
18 Radiocarbon (<sup>14</sup>C) anomalies in eastern North Pacific sediments suggest a significant release of  
19 geologic <sup>14</sup>C-free carbon at the end of the last ice age but without evidence of ocean  
20 acidification. Using inverse carbon cycle modeling optimized with reconstructed atmospheric  
21 CO<sub>2</sub> and <sup>14</sup>C/C, we develop first-order constraints on geologic carbon and alkalinity release over  
22 the last 17.5 thousand years. We construct scenarios allowing the release of 850-2400 Pg C, with  
23 a maximum release rate of 1.3 Pg C yr<sup>-1</sup>, all of which require an approximate equimolar  
24 alkalinity release. These neutralized carbon addition scenarios have minimal impacts on the  
25 simulated marine carbon cycle and atmospheric CO<sub>2</sub>, thereby demonstrating safe and effective  
26 ocean carbon storage. This deglacial phenomenon could serve as a natural analog to the  
27 successful implementation of gigaton-scale ocean alkalinity enhancement, a promising marine  
28 carbon dioxide removal method.

## 29 **Plain language summary**

30 The ocean is the largest carbon reservoir on Earth's surface and, as such, it controls the  
31 concentration of the greenhouse gas carbon dioxide (CO<sub>2</sub>) in the atmosphere over long time  
32 periods. When CO<sub>2</sub> was rising at the end of the last ice age, marine sediment evidence indicates a  
33 regional carbon release into the ocean, due to a distinct carbon isotope fingerprint left behind.  
34 Using a carbon cycle model and atmospheric data, we simulated different geologic carbon addition  
35 scenarios since the last ice age. We find that substantial carbon addition to the ocean could have  
36 occurred (up to 1.3 billion tons per year) without causing significant changes to the carbon cycle,  
37 but only if the carbon is neutralized by alkalinity in an approximate 1:1 ratio. This neutralized  
38 release is similar to an approach of carbon removal called ocean alkalinity enhancement (OAE),  
39 which aims to reduce atmospheric CO<sub>2</sub> as a potential solution for climate change. These findings  
40 suggest that neutralized carbon addition—in the form of “neutralized” bicarbonate ion (HCO<sub>3</sub><sup>-</sup>)  
41 instead of “acidic” CO<sub>2</sub>—could explain the low levels of radiocarbon during the last deglaciation  
42 and shows that large-scale OAE is feasible without causing major changes to the marine carbon  
43 cycle.

## 44 **1 Introduction**

45 Global climate, the global carbon cycle, and the atmospheric concentration of the greenhouse gas  
46 carbon dioxide (CO<sub>2</sub>) have been tightly coupled over recent ice age cycles (Siegenthaler et al.,  
47 2005), including the relatively abrupt ice age terminations and deglacial periods (Marcott et al.,  
48 2014; Shakun et al., 2012). Coupled changes in deep ocean circulation, polar ocean biological  
49 nutrient consumption, and air-sea CO<sub>2</sub> exchange are thought to be the dominate drivers of the  
50 observed CO<sub>2</sub> change (Khaliwala et al., 2019; Rafter et al., 2022; Sigman et al., 2021), but changes  
51 in land carbon storage and seafloor carbon burial in direct response to climate change are also  
52 clearly implicated (Cartapanis et al., 2018; Joos et al., 2001; Köhler et al., 2014). The primary  
53 challenge to all these hypotheses comes from unexplained “anomalies” in the radiocarbon (<sup>14</sup>C)  
54 content within marine foraminifera during deglacial CO<sub>2</sub> rise in the atmosphere, between about  
55 18,000 and 11,500 years before present (18-11.5 thousand years before present or kyr BP, Fig. 1).  
56 These deglacial records of <sup>14</sup>C depletion (decay-corrected <sup>14</sup>C:<sup>12</sup>C ratio, expressed as Δ<sup>14</sup>C; Stuiver  
57 & Polach, 1977) have been uncovered throughout the intermediate-depth (>500m & <1000m)

58 eastern tropical North Pacific (ETNP) Ocean (Lindsay et al., 2016; Marchitto et al., 2007; Rafter  
 59 et al., 2018, 2019; Stott et al., 2009); associated with the weakly ventilated Pacific shadow zone  
 60 (Gehrie et al., 2006; Holzer et al., 2021)

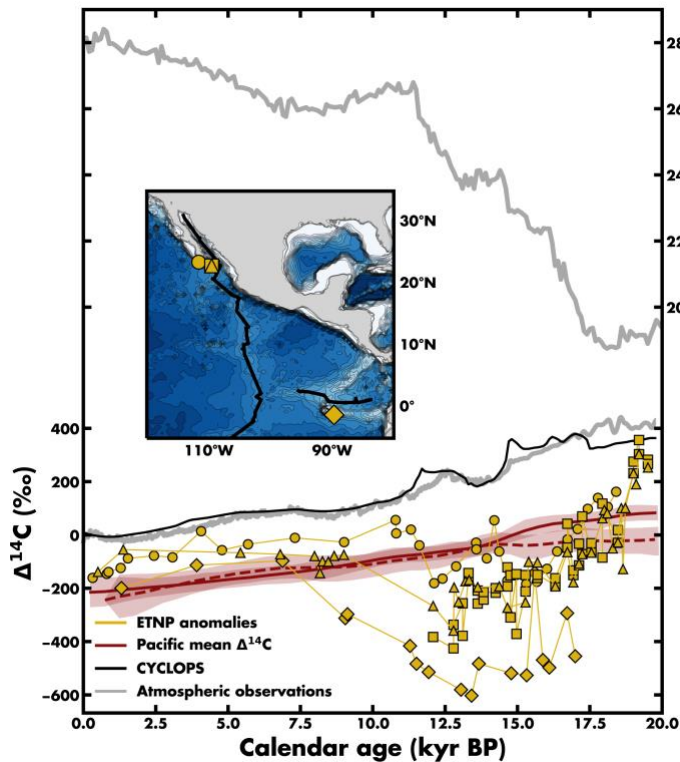


**Figure 1. Unexplained  $\Delta^{14}\text{C}$  anomalies from the intermediate-depth (>500m & <1000m) eastern tropical North Pacific (ETNP). The ETNP anomalies shown are foraminifera from Marchitto et al. (2007) (benthic; circles), Stott et al. (2009) (benthic; diamonds), and Rafter et al. (2018) (squares for benthic, triangles for planktic). The ETNP anomalies are compared with compilation means from the Pacific (red lines; Rafter et al., 2022). Solid and dashed lines represent mid-depth and bottom water, respectively, with red shading denoting the 95% confidence interval. The atmospheric  $\Delta^{14}\text{C}$  for our CYCLOPS control simulation is shown as a solid black line. Reconstructed atmospheric  $\Delta^{14}\text{C}$  (Reimer et al., 2020) and  $\text{CO}_2$**

82 (Bereiter et al. 2015) are shown in gray. Individual  $\Delta^{14}\text{C}$  records are positioned on the map, with  
 83 ocean bathymetry and the East Pacific Rise spreading center (black lines).

84 These regional depletions in seawater  $\Delta^{14}\text{C}$  were initially attributed to a release of dissolved  
 85 inorganic carbon (DIC) that had been sequestered for thousands of years in the abyssal ocean,  
 86 hinting at deglacial changes in ocean circulation (Bova et al., 2018; Broecker, 2009; Broecker &  
 87 Barker, 2007; Marchitto et al., 2007). However, this ocean release interpretation has two main  
 88 shortcomings (Hain et al., 2011): (a) the Last Glacial Maximum (LGM) deep ocean was not  
 89 sufficiently  $^{14}\text{C}$ -depleted (dashed red line in Fig. 1) to be the source of the mid-depth anomalies,  
 90 and (b) once the isotopic signature of anomalously  $^{14}\text{C}$ -depleted carbon is transported to the mid-  
 91 depth Pacific it would rapidly dissipate into the global carbon cycle via ocean circulation and air-  
 92 sea gas exchange. This hypothesis is further contradicted by a new compilation showing no  
 93 appreciable  $^{14}\text{C}$ -depletion at any depth for the basin-scale Pacific during the deglaciation (red lines  
 94 in Fig. 1; Rafter et al., 2022), as would be required if the abyssal ocean caused the ETNP  $^{14}\text{C}$   
 95 anomalies. Additionally, deep-sea coral  $^{14}\text{C}$  records from the Galápagos with excellent age model  
 96 controls (Chen et al., 2020) and South Pacific  $^{14}\text{C}$  records bathed in modern Antarctic Intermediate  
 97 Water (De Pol-Holz et al., 2010; Rose et al., 2010; Siani et al., 2013; Zhao & Keigwin, 2018) show  
 98 no  $^{14}\text{C}$ -depletion comparable to the ETNP anomalies. This lack of basin-wide mid-depth  $\Delta^{14}\text{C}$   
 99 depletion is an important observational constraint we will consider below.

100 An alternative set of proposals suggest these anomalously low  $\Delta^{14}\text{C}$  values reflect an addition of  
 101  $^{14}\text{C}$ -free carbon from a geologic source (Stott et al., 2009; Stott & Timmermann, 2011; Ronge et  
 102 al., 2016; Rafter et al., 2018, 2019; Skinner & Bard, 2022). A common objection to this hypothesis

103 is the potential for ocean acidification, which would contradict the evidence of ETNP carbonate  
104 preservation during the last deglacial (Lindsay et al., 2015; Marchitto et al., 2007; Ortiz et al.,  
105 2004; Rafter et al., 2019; Skinner & Bard, 2022; Stott et al., 2009). However, if the geologic carbon  
106 addition was neutralized by a commensurate influx of alkalinity—e.g., carbon introduced in the  
107 form of “neutralized” bicarbonate ion instead of “acidic” CO<sub>2</sub>—there would be muted effects on  
108 seawater pH, CaCO<sub>3</sub> burial, and atmospheric CO<sub>2</sub> (Rafter et al., 2019).

109 Neutralized <sup>14</sup>C-free carbon could be generated within marine sediments via metamorphic or  
110 hydrothermal processes (Rafter et al., 2019; Skinner & Bard, 2022). Subsequently, it would be  
111 transported and dispersed throughout the ocean and atmosphere, leading to the dilution of the  
112 atmospheric <sup>14</sup>C reservoir and a reduction of atmospheric Δ<sup>14</sup>C. Most of the decline in atmospheric  
113 Δ<sup>14</sup>C during the last deglaciation can be explained by Southern Ocean CO<sub>2</sub> release, Atlantic  
114 circulation changes, and the decline in cosmogenic <sup>14</sup>C production driven by a strengthening of  
115 Earth’s magnetic field (black line in Fig. 1; Hain et al., 2014; Skinner & Bard, 2022), leaving  
116 limited opportunities in the planetary <sup>14</sup>C budget for the addition of <sup>14</sup>C-free geologic carbon.

117 This study presents the first carbon cycle model results that investigate the possibility of coupled  
118 geologic carbon and alkalinity release during the last deglaciation. Our experiments build on the  
119 deglacial model scenario of Hain et al. (2014) and test the sensitivity of our results to changes in  
120 terrestrial carbon storage. We use a stepwise numerical model optimization method that assimilates  
121 observed atmospheric CO<sub>2</sub> and Δ<sup>14</sup>C data to find the internally consistent rates of geologic carbon  
122 and alkalinity release, permafrost carbon destabilization, and land biosphere regrowth. This is  
123 intended to raise important research questions relevant to different fields of research: can seafloor  
124 spreading centers respond to climate change? What subsurface processes could mobilize carbon  
125 and alkalinity at relevant specific rates? And do deglacial radiocarbon anomalies provide a natural  
126 analog for purposeful ocean alkalinity enhancement (OAE) as a means of marine carbon dioxide  
127 removal (mCDR) (Bach & Boyd, 2021; NASEM, 2022)?

## 128 **2 Materials and Methods**

129 Motivated by the regional ETNP anomalies (Fig. 1), we use the CYCLOPS global carbon cycle  
130 model (Hain et al., 2010, 2011, 2014; Keir, 1988; see supplementary material, SM, for model  
131 configuration) to simulate the flux of geologic carbon from Pacific mid-ocean ridge systems. This  
132 involves four experiments, progressively adding optimized open-system carbon and alkalinity  
133 fluxes, along with an imposed initial <sup>14</sup>C inventory change (top row of Fig. 2): (1) We invert for  
134 the optimal rates of carbon and alkalinity release to the intermediate-depth (200m-1500m) North  
135 Pacific region of the model (experiment NP); (2) We add the possibility of land carbon uptake to  
136 the optimization (experiment NP+LC); (3) We include the release of <sup>14</sup>C-free permafrost carbon  
137 to the atmosphere (experiment NP+LC+PF); and (4) We adjust the initial LGM <sup>14</sup>C inventory by  
138 +3.5% to account for the uncertain history of Earth’s magnetic field, <sup>14</sup>C production, and  
139 reconstructed Δ<sup>14</sup>C near the LGM (Fig 3a, Dinauer et al., 2020; Roth & Joos, 2013) (experiment  
140 NP+LC+PF+RC).

141 All experiments include the identical background forcings of the control run, based on the deglacial  
142 carbon cycle scenario from Hain et al. (2014). Although this is an idealized model scenario, we  
143 use it as our starting point because the LGM carbon cycle forcing of CYCLOPS is well  
144 documented (Hain et al., 2010) and consistent with reconstructed surface ocean pH changes (Chalk  
145 et al., 2017; Hain et al., 2018). Additionally, the deglacial model scenario agrees reasonably well

146 with subsequent  $^{14}\text{C}$  measurements and data compilations (Zhao et al., 2018; Rafter et al., 2022),  
 147 as shown by the direct comparison for the Pacific and for all other basins (Fig. S1). More in-depth  
 148 descriptions of each experiment can be found in the SM.

149 For all experiments, the optimized open-system carbon and alkalinity fluxes were determined by  
 150 a numerical algorithm that minimizes the deviation between simulated atmospheric  $\text{CO}_2$  ( $\text{CO}_2^{\text{model}}$ )  
 151 and  $\Delta^{14}\text{C}$  ( $\Delta^{14}\text{C}^{\text{model}}$ ), compared to reconstructed atmospheric  $\text{CO}_2$  ( $\text{CO}_2^{\text{obs}}$ ) from the most recent  
 152 compilation of Antarctic ice core  $\text{CO}_2$  data (Bereiter et al., 2015) and  $\Delta^{14}\text{C}$  ( $\Delta^{14}\text{C}^{\text{obs}}$ ) from IntCal20  
 153 (Reimer et al., 2020). The algorithm's objective function  $f$  is scaled to the 90ppm  
 154 glacial/interglacial  $\text{CO}_2$  range and the  $\sim 250\text{‰}$  atmospheric  $\Delta^{14}\text{C}$  change after accounting for  
 155 Earth's magnetic field strengthening:

$$156 \quad f(\text{CO}_2, \Delta^{14}\text{C}) = \frac{|\text{CO}_2^{\text{obs}} - \text{CO}_2^{\text{model}}|}{90 \text{ ppm}} + \frac{|\Delta^{14}\text{C}^{\text{obs}} - \Delta^{14}\text{C}^{\text{model}}|}{250 \text{ ‰}}$$

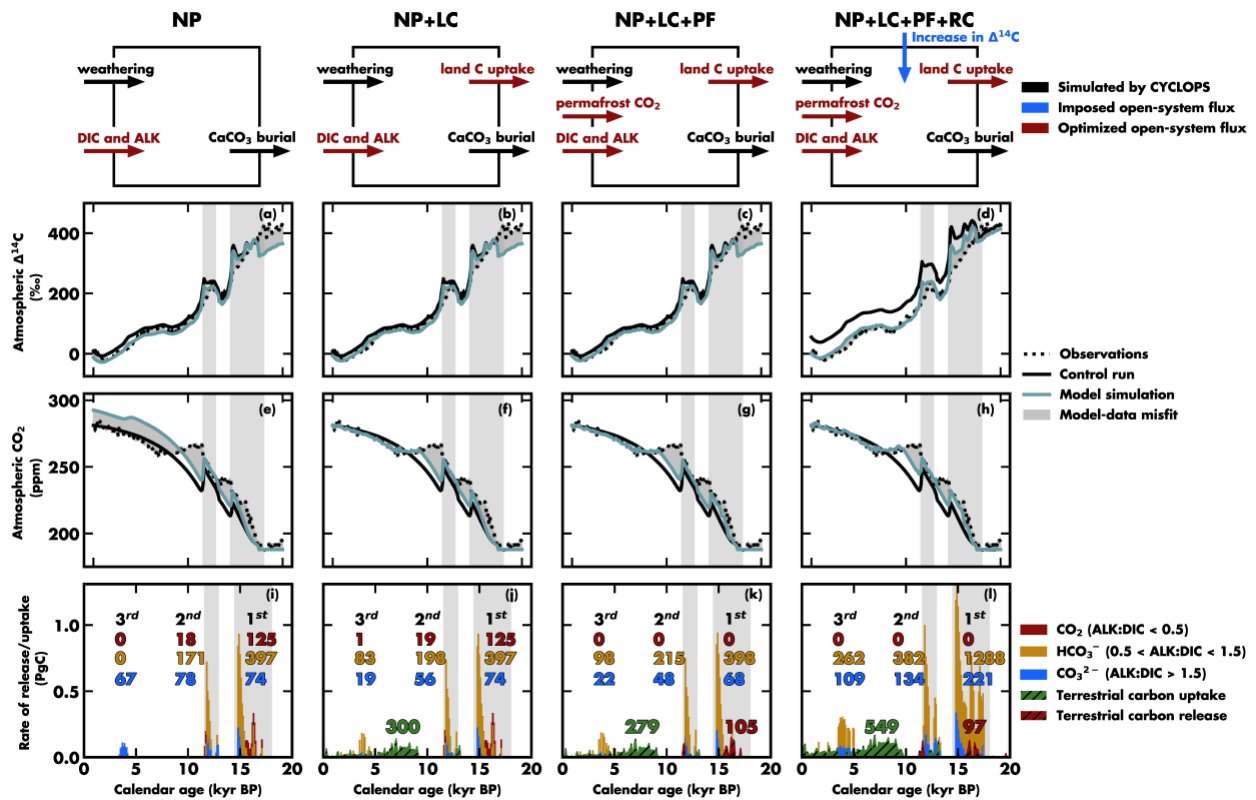
157 We do not permit unrealistic 'negative' geologic fluxes, permafrost growth, or land carbon  
 158 contraction that could otherwise help the model align with the observations. For experiments that  
 159 include land carbon uptake, we included a deliberate heuristic favoring land carbon uptake during  
 160 the Holocene. If  $\text{CO}_2^{\text{model}}$  was greater than  $\text{CO}_2^{\text{obs}}$  and the atmospheric  $\Delta^{14}\text{C}$  model-data misfit was  
 161 less than 20‰, then the optimized carbon flux is added to the terrestrial biosphere rather than the  
 162 intermediate-depth North Pacific (with an alkalinity flux of zero). For experiments that include  
 163 carbon release from permafrost destabilization, the optimized flux is only activated when the  
 164 optimization algorithm would otherwise add  $\text{CO}_2$  (ALK-to-DIC < 0.5) into the intermediate-depth  
 165 North Pacific, instead releasing the equivalent amount of  $\text{CO}_2$  directly to the atmosphere. Further  
 166 details of the algorithm can be found in the SM.

## 167 **3 Results**

### 168 **3.1 Atmospheric constraints on geologic carbon addition**

169 All four simulations improve the overall  $\text{CO}_2$  and  $\Delta^{14}\text{C}$  model-data misfit compared to the control  
 170 run (blue vs. black line, Fig. 2). This model-data misfit is progressively minimized as more open-  
 171 system carbon and alkalinity fluxes are added to the model, with the NP+LC+PF+RC simulating  
 172 the smallest model-data misfit. Each simulation has two main pulses of geologic carbon during the  
 173 deglaciation and one smaller pulse during the Holocene. Our optimization triggers these geologic  
 174 pulses when  $\Delta^{14}\text{C}^{\text{model}}$  rises above  $\Delta^{14}\text{C}^{\text{obs}}$ , which we call  $^{14}\text{C}$  opportunities. Most of the geologic

175 carbon is added as bicarbonate ion (61-84%, Table S1), with net ALK-to-DIC ratios between 1.08  
 176 and 1.19 (Table S1) across all four simulations.



177

178 **Figure 2. Simulated atmospheric response to optimized geologic carbon release scenarios.**  
 179 Schematic representation of experimental setups depicting the progressive addition of optimized  
 180 and imposed open-system fluxes (colored arrows) (top row). Subsequent rows illustrate simulation  
 181 results for atmospheric  $\Delta^{14}\text{C}$  (a-d), atmospheric  $\text{CO}_2$  (e-h), and carbon release/uptake rates (i-l).  
 182 In panels i-l, colored numbers represent the amounts of  $\text{CO}_2$  (red),  $\text{HCO}_3^-$  (yellow), and  $\text{CO}_3^{2-}$   
 183 (blue) released with each geologic carbon pulse. Similarly, terrestrial carbon uptake is shown in  
 184 green, and terrestrial carbon release is in red, all in units of Pg C. Gray bars denote Heinrich  
 185 Stadial 1 and Younger Dryas, while model-data misfit is shaded in gray.

186 For our first three experiments (NP, NP+LC, NP+LC+PF)—which include no adjustment to the  
 187 initial  $^{14}\text{C}$  inventory—a total of 846-929 Pg C geologic carbon was added over the 20-kyrs (Table  
 188 S1), with peak rates as large as  $0.9 \text{ Pg C yr}^{-1}$  (Fig 2i-k) during the first pulse of addition ( $\sim 15$ -kyr  
 189 BP). Of those experiments that included terrestrial regrowth (NP+LC, NP+LC+PF), between 279-  
 190 300 Pg C (Table S1) of simulated carbon uptake occurs, mainly during the Holocene. When we  
 191 include terrestrial carbon release from permafrost thaw (NP+LC+PF), 105 Pg C (Fig 2k, Table S1)  
 192 is released around 16-kyr BP during the first pulse of carbon addition. Our fourth experiment,  
 193 NP+LC+PF+RC, includes an adjusted  $^{14}\text{C}$  inventory at the LGM initial state alongside all the  
 194 above open-system fluxes. The higher initial  $\Delta^{14}\text{C}^{\text{model}}$  increases the opportunity for the subsequent  
 195 addition of  $^{14}\text{C}$ -free carbon, leading to a greater amount of total carbon added (2396 Pg C, Table

196 S1), higher release rates (up to 1.3 Pg C yr<sup>-1</sup>, Fig. 2f), more land carbon uptake (550 Pg C; Table  
 197 S1), but a similar carbon release from permafrost thaw around 16-kyr BP (97 Pg C).

### 198 3.2 Regional and bulk ocean impacts from large-scale geologic carbon addition

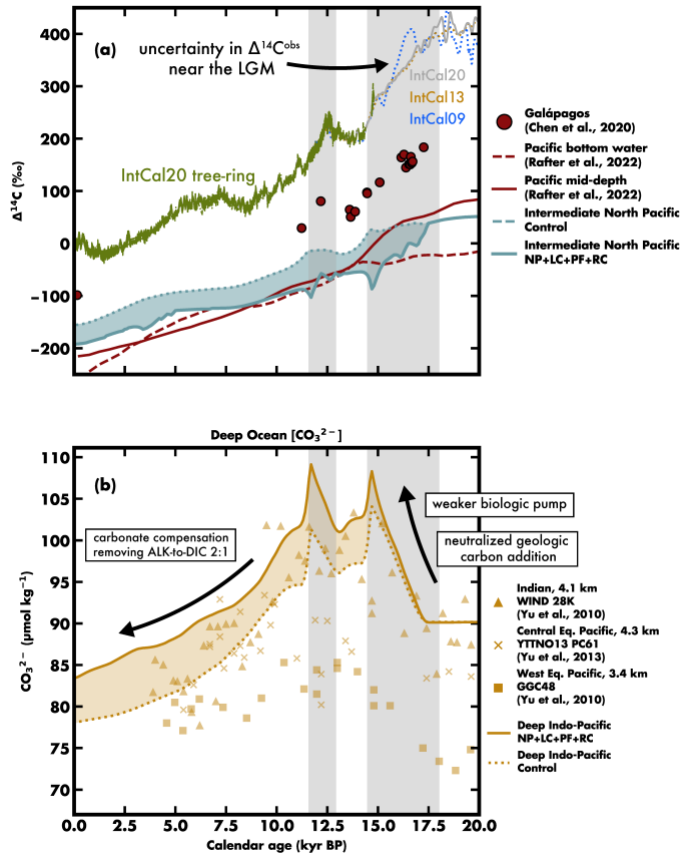


*Figure 3. Neutralized carbon release has limited impacts on basin scale  $\Delta^{14}\text{C}$  and deep ocean  $[\text{CO}_3^{2-}]$ . In Panel a, NP+LC+PF+RC drives mild  $\Delta^{14}\text{C}$  depletion from the control run (shaded blue area), consistent with various datasets: deep-sea coral near the Galápagos (red circles), mean  $\Delta^{14}\text{C}$  from Pacific mid-depth and bottom water (solid and dashed red line), and atmospheric  $\Delta^{14}\text{C}$  (solid gray and green, dotted yellow and blue). Noteworthy is the  $\Delta^{14}\text{C}$  disagreement near the LGM in the last three IntCal iterations, converging with tree-ring data availability (solid green line). Panel b illustrates NP+LC+PF+RC causing an increase in  $[\text{CO}_3^{2-}]$  in the Indo-Pacific deep ocean compared to the control run (shaded yellow). Simulated  $[\text{CO}_3^{2-}]$  align broadly with observations from the Indian (yellow triangle) and Equatorial Pacific (yellow square and X). Gray bars represent Heinrich Stadial 1 and Younger Dryas.*

222

223 The most severe carbon cycle impacts should arise during our largest geologic carbon addition  
 224 scenario (NP+LC+PF+RC). However, only minor  $\Delta^{14}\text{C}$  anomalies are simulated in the  
 225 intermediate-depth North Pacific box where the carbon is released (solid blue line, Fig. 3a).  
 226 Consequently, the simulated intermediate-depth North Pacific  $\Delta^{14}\text{C}$  is in broad agreement with the  
 227 mean  $\Delta^{14}\text{C}$  from the mid-depth (neutral density of 27.5–28 kg m<sup>-3</sup>) Pacific, calculated from a new  
 228 proxy <sup>14</sup>C/C compilation (red line in Fig. 3a, Rafter et al., 2022). Given that the present-day mid-  
 229 depth Pacific contains the oldest waters in the entire ocean, it serves as a conservative benchmark  
 230 for comparing our simulated intermediate-depth results. Furthermore, the lack of severe  $\Delta^{14}\text{C}$   
 231 depletion in the NP+LC+PF+RC simulation is supported by a deep-sea coral record considered  
 232 representative of the <sup>14</sup>C content of intermediate waters near the Galápagos islands (red circles in  
 233 Fig. 3a, Chen et al., 2020).

234 Similarly, we find limited impacts on deep ocean  $[\text{CO}_3^{2-}]$ —which largely determines CaCO<sub>3</sub>  
 235 saturation and thus CaCO<sub>3</sub> burial—when the geologic carbon is added as HCO<sub>3</sub><sup>-</sup> (ALK-to-DIC~1).  
 236 This is clear from Fig. 3b, as the NP+LC+PF+RC only simulates a moderate increase (~5 μmol  
 237 kg<sup>-1</sup>) in deep-ocean  $[\text{CO}_3^{2-}]$  compared to the control simulation. With a deglacial increase in deep-  
 238 ocean  $[\text{CO}_3^{2-}]$  due to a weakened biological pump and a subsequent decrease in deep-ocean  $[\text{CO}_3^{2-}]$

239 ] from carbonate compensation, both the control and NP+LC+PF+RC simulation broadly follow  
240  $[\text{CO}_3^{2-}]$  observations (Yu et al., 2010, 2013).

241 In addition to  $\Delta^{14}\text{C}$  impacts, geologic carbon will impact the ocean's stable isotope ratio of carbon  
242 ( $^{13}\text{C}/^{12}\text{C}$ , reported as  $\delta^{13}\text{C}$ ), but this ultimately depends on the source. We run an additional set of  
243 experiments by calculating the bulk ocean  $\delta^{13}\text{C}$  change for two endmember sources of neutralized  
244 geologic carbon (described in SM): bicarbonate from anaerobic oxidation of thermogenic methane  
245 (AOM; Rafter et al., 2019) and geologic  $\text{CO}_2$  neutralized by carbonate dissolution (Skinner &  
246 Bard, 2022), with  $\delta^{13}\text{C}$  values of  $-25\text{‰}$  and  $-2.5\text{‰}$ , respectively. When 2400 Pg C is added (as  
247 suggested by our NP+LC+PF+RC experiment), we simulate bulk  $\delta^{13}\text{C}$  ocean changes of  $-1.5\text{‰}$   
248 for AOM and  $-0.2\text{‰}$  for carbonate dissolution. Given that reconstructed oceanic  $\delta^{13}\text{C}$  values have  
249 not fluctuated more than  $\sim 1\text{‰}$  over the last 800-kyrs (Hodell et al., 2003), our simulations suggest  
250 geologic carbon from a methane source ( $\delta^{13}\text{C} \leq -25\text{‰}$ ) is unlikely for our extreme carbon addition  
251 scenario of 2400 Pg C. Considering the decoupled nature of neutralized geologic carbon addition  
252 and atmospheric  $\text{CO}_2$ , along with the limited impact on basin-scale  $\Delta^{14}\text{C}$ , deep ocean  $[\text{CO}_3^{2-}]$ , and  
253 bulk ocean  $\delta^{13}\text{C}$ , these findings underscore that the global  $^{14}\text{C}$  budget is the strongest constraint  
254 available for assessing geologic carbon addition at the global scale.

## 255 **4 Discussion**

256 The core outcome of our study is that atmospheric  $\text{CO}_2$  and  $\text{CaCO}_3$  burial are effectively blind to  
257 carbon release neutralized by alkalinity in a ratio near 1:1, with the timely implication that ocean  
258 alkalinity enhancement may be an effective pathway for the mitigation of anthropogenic carbon  
259 emissions (NASEM, 2022). In the specific context of the deglacial period, this insensitivity allows  
260 for large-scale geologic carbon addition scenarios constrained most directly by the planetary  
261 radiocarbon budget, as long as there was concomitant natural ocean alkalinity enhancement.  
262 Additionally, our most extreme carbon addition scenario is insufficient to drive significant  $\Delta^{14}\text{C}$   
263 depletion across the North Pacific, in agreement with observations representative of the North  
264 Pacific and Pacific basins. This supports the idea that the enigmatic  $\Delta^{14}\text{C}$  anomalies of the ETNP  
265 are likely regional or localized phenomena that could be exploited to derive a set of local  
266 constraints on possible carbon and alkalinity release that would be completely independent from  
267 the global  $\text{CO}_2$  and  $^{14}\text{C}$  budget constraints used in this study.

### 268 **4.1 Large amounts of bicarbonate allowable**

269 We optimized our carbon cycle modeling simulations, which include different open-system fluxes  
270 and changes to the  $^{14}\text{C}$  inventory, with the addition of geologic carbon. The simulations show that  
271 up to 2397 Pg of geologic carbon, mainly as bicarbonate ion, can be consistent with the observed  
272 deglacial changes in atmospheric  $\text{CO}_2$  and  $\Delta^{14}\text{C}$ . Due to the alkalinity accompanying DIC during  
273 bicarbonate addition, geologic carbon in this form can be added at rates as large as  $1.3 \text{ Pg C yr}^{-1}$   
274 (Fig. 2l) with limited impacts on atmospheric  $\text{CO}_2$  and deep-sea  $[\text{CO}_3^{2-}]$ .

275 Prior work has estimated that deglacial geologic  $\text{CO}_2$  emissions from mantle decompression could  
276 have reached up to  $0.2 \text{ Pg C yr}^{-1}$  (Cartapanis et al., 2018; Roth & Joos, 2012), much smaller than  
277 our maximum yearly rates. However, these lower rates were derived assuming the geologic carbon  
278 came only as  $\text{CO}_2$  rather than as bicarbonate ion. When carbon is added without alkalinity (i.e.,  
279  $\text{CO}_2$ ), atmospheric  $\text{CO}_2$  and  $\text{CaCO}_3$  burial constraints are highly sensitive to any carbon added to

280 the system. However, when adding neutralized carbon (bicarbonate), atmospheric CO<sub>2</sub> and CaCO<sub>3</sub>  
281 burial constraints become effectively blind to the carbon release, no longer constraining the carbon  
282 release rate or total. During bicarbonate addition, the constraining factor shifts to the planetary <sup>14</sup>C  
283 mass balance and its reflection in the atmospheric Δ<sup>14</sup>C record (via IntCal20, Reimer et al., 2020),  
284 which can indirectly record the dilution of <sup>14</sup>C-enriched environmental carbon by <sup>14</sup>C-free geologic  
285 carbon. This Δ<sup>14</sup>C<sup>obs</sup> constraint on bicarbonate release leads to an upper bound of 800-1000 Pg C  
286 in our first three simulations (NP, NP+LC, NP+LC+PF)—a 2-2.5% increase of total ocean carbon  
287 inventory. Furthermore, if we take into consideration the uncertainty in the planetary <sup>14</sup>C mass  
288 balance (Dinauer et al., 2020; Roth & Joos, 2013) by increasing the initial LGM <sup>14</sup>C inventory by  
289 3.5%, the opportunity for subsequent geologic carbon release increases to ~2500 Pg C (6.5%  
290 increase of total ocean carbon inventory). In other words, a higher initial LGM <sup>14</sup>C/C can  
291 substantially increase the opportunity for <sup>14</sup>C-free geologic carbon release since the LGM.

292 Considering the idealized nature of our experiments and because of biases inherited from our  
293 control run (Hain et al., 2014), our optimization results should not be taken as estimates of geologic  
294 carbon release or of other simulated open-system carbon fluxes (e.g., LC, PF). Instead, we argue  
295 that geologic carbon release greater than 800-1000 Pg C is rendered unlikely, and release of greater  
296 than 2400 Pg C is implausible in the face of Δ<sup>14</sup>C<sup>obs</sup>. Further, if indeed there was substantial  
297 geologic carbon release since the LGM, it must have been in the neutralized form of bicarbonate  
298 ion with a net ALK-to-DIC ratio near 1, as proposed by Rafter et al. (2019), to avoid violating  
299 constraints from atmospheric CO<sub>2</sub> and CaCO<sub>3</sub> burial. Therefore, we argue that geologic carbon  
300 release played only a minor role in raising CO<sub>2</sub> at the end of the last ice age, even if the total  
301 amount of carbon release was substantial. This contrasts with prior deglacial geologic carbon  
302 addition research, which attributes glacial/interglacial CO<sub>2</sub> variability to liquid CO<sub>2</sub> release (Stott  
303 et al., 2019; Stott & Timmermann, 2011).

#### 304 **4.2 Geologic carbon as an explanation for Δ<sup>14</sup>C anomalies?**

305 When first discovered, the Δ<sup>14</sup>C anomalies in the ETNP were taken to be the signature of carbon  
306 release from the deep ocean to the atmosphere (Marchitto et al., 2007). This earlier view of the  
307 Δ<sup>14</sup>C anomalies buttresses the longstanding notion that stagnation of deep ocean circulation during  
308 the LGM created an isolated <sup>14</sup>C-deplete reservoir for the sequestration of atmospheric CO<sub>2</sub>  
309 (Broecker & Barker, 2007; Skinner et al., 2010)—and this view remains prevalent (e.g., Bova et  
310 al., 2018). However, deep ocean carbon storage and its effect on atmospheric CO<sub>2</sub> is more closely  
311 tied to the degree of nutrient consumption in the polar ocean regions that form new deep water  
312 (Hain et al., 2010, 2014; Ito & Follows, 2005; Marinov et al., 2008a, 2008b; Sigman et al., 2010,  
313 2021; Sigman & Haug, 2003) rather than being a simple function of the rate of deep ocean  
314 overturning. Further, a new compilation of global ocean Δ<sup>14</sup>C records reveals that the LGM <sup>14</sup>C  
315 age of the global deep ocean was about ~1000 years greater than today (Rafter et al., 2022),  
316 sufficient to explain a large portion of the observed Δ<sup>14</sup>C<sup>obs</sup> decline during the deglacial period  
317 (Broecker & Barker, 2007; Hain et al., 2014), but not nearly <sup>14</sup>C-deplete enough to produce the  
318 ETNP Δ<sup>14</sup>C anomalies (Fig. 3a). Rather than becoming a plank in our evolving understanding of  
319 coupled glacial/interglacial changes in ocean circulation and the global carbon cycle, the existence  
320 of these Δ<sup>14</sup>C anomalies has become its own vexing problem, defying conventional explanations  
321 based on ocean circulation.

322

323 There are numerous reasons why a given sample would yield an anomalously low reconstructed  
324  $^{14}\text{C}/\text{C}$ , but the spatial-temporal clustering of  $^{14}\text{C}$  anomalies in the upper 1 km of the ETNP water  
325 column is remarkable (e.g., Bova et al., 2018; Lindsay et al., 2015; Marchitto et al., 2007; Rafter  
326 et al., 2018, 2019; Stott et al., 2019), especially when contrasted with nearby records that broadly  
327 track atmospheric  $^{14}\text{C}$  change without discernible  $^{14}\text{C}$  anomalies (e.g., Bova et al., 2018; Chen et  
328 al., 2020; De Pol-Holz et al., 2010; Rose et al., 2010; Siani et al., 2013; Zhao & Keigwin, 2018).  
329 Previous modeling of the problem suggests that any  $^{14}\text{C}$  anomaly in the upper ocean would rapidly  
330 dissipate by ocean circulation and air-sea gas exchange (Hain et al., 2011) such that upper ocean  
331  $\Delta^{14}\text{C}$  is expected to track atmospheric  $\Delta^{14}\text{C}$  change since the LGM (Hain et al., 2014), as is  
332 observed in independently dated coral  $^{14}\text{C}$  records from the Atlantic and Pacific (e.g., Chen et al.,  
333 2020) and other records outside the anomalous ETNP cluster. Our new results advance the  
334 argument by demonstrating that even the release of  $>2000$  Pg C is insufficient to generate a  
335 significant  $^{14}\text{C}$  anomaly on the basin scale resolved in our current model (Fig. 3a), related to the  
336 rapid global dissipation of  $^{14}\text{C}$  isotope anomalies in the global carbon cycle (Hain et al., 2011).  
337 That is, the absence of anomalies in most upper ocean  $^{14}\text{C}$  reconstructions are normal and expected  
338 even in the case of substantial simulated carbon release. The caveat to the argument is that a small  
339  $\Delta^{14}\text{C}$  reduction simulated at the basin scale would be consistent with a severe  $^{14}\text{C}$  anomaly  
340 concentrated in a small sub-region, such as observed in the ETNP.

341  
342 The  $^{14}\text{C}$  anomalies of the ETNP may record carbon release associated with processes linked to  
343 spreading centers separating the Cocos, Nazca, and Pacific plates that produce very high regional  
344 geothermal heat flux ( $>0.1$  W  $\text{m}^{-2}$  throughout the region; Pollack et al., 1993). While we cannot  
345 usefully comment on whether these geologic systems are dynamic enough to yield defined pulses  
346 of carbon release, our results highlight that only a neutralized form of carbon release would be  
347 consistent with the atmospheric  $\text{CO}_2$  constraint and observations of good (sometimes improved)  
348 seafloor carbonate preservation (Fig. 3b; Yu et al., 2008, 2010, 2013) during the main purported  
349 geologic carbon pulses. Indeed, the temporal coincidence of the  $^{14}\text{C}$  anomalies with  
350 stadial/interstadial climate change, deglacial ocean heat uptake (Poggemann et al., 2018), and  
351 circulation change (e.g., McManus et al., 2004; Rafter et al., 2022) may point to a climatic or  
352 environmental trigger of carbon release, rather than a being a purely stochastic volcanogenic  
353 phenomenon.

354  
355 However, why would severe  $^{14}\text{C}$  anomalies persist for millennia in the ETNP upper ocean water  
356 column if ocean circulation and air-sea gas exchange act to rapidly dissipate the anomalous carbon  
357 globally (Hain et al., 2011)? We propose two alternative resolutions that we cannot distinguish  
358 based on our current model and existing data: Either the anomalies are localized and reflect  
359 geologic carbon diffusion out of the underlying sediment stack rather than bottom water  $\Delta^{14}\text{C}$ , or  
360 the anomalies are regional and reflect the accumulation of geologic carbon in the ETNP shadow  
361 zone of ocean circulation with a sharp and persistent chemical gradient to the open ocean mid-  
362 depth Pacific.

363  
364 If the anomalies are localized, we might expect each anomalous record to differ in magnitude and  
365 timing. Finding individual mid-depth sites in the ETNP where  $^{14}\text{C}$  anomalies are missing (e.g.,  
366 Bova et al., 2018; Chen et al., 2020) alongside records with  $^{14}\text{C}$  anomalies that are only broadly  
367 similar, would tend to support the localized explanation. Conversely, if geologic carbon were  
368 added to a dynamically isolated region, such as the upper ocean ETNP (Margolskee et al., 2019),

369 then seawater  $\Delta^{14}\text{C}$  might diverge substantially from the  $\Delta^{14}\text{C}$  of the open Pacific and atmosphere.  
370 However, that regional signal would need to be shared by all radiocarbon records in the  
371 hydrodynamic region (cf. Chen et al., 2020). If the anomalies did reflect the restricted regional  
372 ocean circulation of the ETNP, it would seem plausible that the carbon release mechanism also  
373 operated in regions outside the ETNP (e.g., Bryan et al., 2010).

## 374 **5 Conclusion**

375 We document a set of carbon cycle model scenarios since the LGM that include substantial (800-  
376 2400 Pg C) release of geologic carbon broadly consistent with reconstructed atmospheric  $\text{CO}_2$  rise,  
377  $\Delta^{14}\text{C}$  decline, and  $\text{CaCO}_3$  burial patterns. In all simulations, geologic carbon release is primarily  
378 released as bicarbonate ion (i.e., with a DIC:ALK near 1), with minimal effect on the marine  
379 carbon cycle and atmospheric  $\text{CO}_2$ . That is, we demonstrate the possibility of climate-neutral  
380 geologic carbon and alkalinity release during the deglacial period in a way that is consistent with  
381 a dominant Southern Ocean control on climate-carbon coupling over ice age cycles. As such, we  
382 do not prove that such geologic carbon release happened but rather we hope to expand what is  
383 deemed possible. The central outcome of this study is that the deglacial  $\Delta^{14}\text{C}$  anomalies from the  
384 ETNP region may represent a natural analog for the successful application of ocean alkalinity  
385 enhancement (OAE) as a means to neutralize anthropogenic carbon emissions.

386 Introducing geologic carbon will dilute the planetary inventory of cosmogenic radiocarbon ( $^{14}\text{C}$ )  
387 such that the largest release of  $^{14}\text{C}$ -free carbon (2400 Pg C) can reduce the average  $\Delta^{14}\text{C}$  of  
388 environmental carbon by about ~50%. Therefore, the planetary  $^{14}\text{C}$  budget can be used to rule out  
389 the most extreme scenarios for geologic carbon release, offering an upper-bound constraint for  
390 carbon transfers from geologic and terrestrial carbon reservoirs to the ocean/atmosphere carbon  
391 cycle. That is, our model scenarios are designed to explore the limit of what appears to be possible  
392 in the context of global constraints from  $\text{CO}_2$  and  $^{14}\text{C}$  reconstructions. We find that bicarbonate  
393 release was likely limited to less than 1000 Pg C, but when considering uncertainty in the history  
394 of cosmogenic  $^{14}\text{C}$  production, the limit for bicarbonate release may be as high as 2400 Pg C.

395 The spatial cluster of deglacial  $\Delta^{14}\text{C}$  anomalies in the upper water column of the ETNP may be  
396 evidence for geologic carbon release associated with the seafloor spreading center defining the  
397 East Pacific Rise (Fig. 1; (Lindsay et al., 2015; Marchitto et al., 2007; Rafter et al., 2018, 2019;  
398 Stott et al., 2009). Confirming or rejecting this hypothesis would have several implications:  
399 Without large-scale carbon release, we lack an adequate explanation for the ETNP  $\Delta^{14}\text{C}$  anomalies,  
400 suggesting an open gap in our understanding of the  $^{14}\text{C}$ -proxy system used to reconstruct ocean  
401 circulation changes in response to deglacial climate change. Alternatively, with large pulses of  
402 geologic carbon release in the ETNP, we lack an adequate explanation for how bicarbonate is  
403 derived from geologic carbon sources during the deglaciation, suggesting a gap in our

404 understanding of glacial/interglacial changes in seafloor spreading and its role in the global carbon  
405 cycle.

## 406 **Acknowledgments**

407 This research was funded by the National Science Foundation (Collaborative Research Grants  
408 OCE-2032340 to MPH and OCE-2032340 to PAR).

## 409 **Open Research**

410 Detailed model description and configuration are available in the Supporting Information. The  
411 plotting code and simulation results are found on GitHub  
412 (<https://github.com/RyanAGreen/Deglacial-Neutralized-Carbon-14C>) and Zenodo  
413 (<https://zenodo.org/badge/latestdoi/627637425>).

## 414 **References:**

- 415 Bach, L. T., & Boyd, P. W. (2021). Seeking natural analogs to fast-forward the assessment of marine CO<sub>2</sub> removal.  
416 *Proceedings of the National Academy of Sciences*, 118(40), e2106147118.  
417 <https://doi.org/10.1073/pnas.2106147118>
- 418 Bereiter, B., Eggleston, S., Schmitt, J., Nehrbass-Ahles, C., Stocker, T. F., Fischer, H., Kipfstuhl, S., & Chappellaz,  
419 J. (2015). Revision of the EPICA Dome C CO<sub>2</sub> record from 800 to 600 kyr before present. *Geophysical*  
420 *Research Letters*, 42(2), 542–549. <https://doi.org/10.1002/2014GL061957>
- 421 Bova, S. C., Herbert, T. D., & Altabet, M. A. (2018). Ventilation of Northern and Southern Sources of Aged Carbon  
422 in the Eastern Equatorial Pacific During the Younger Dryas Rise in Atmospheric CO<sub>2</sub>. *Paleoceanography*  
423 *and Paleoclimatology*, 33(11), 1151–1168. <https://doi.org/10.1029/2018PA003386>
- 424 Broecker, W. (2009). The Mysterious <sup>14</sup>C Decline. *Radiocarbon*, 51(1), 109–119.  
425 <https://doi.org/10.1017/S0033822200033737>
- 426 Broecker, W., & Barker, S. (2007). A 190‰ drop in atmosphere’s Δ14C during the “Mystery Interval” (17.5 to 14.5  
427 kyr). *Earth and Planetary Science Letters*, 256(1–2), 90–99. <https://doi.org/10.1016/j.epsl.2007.01.015>
- 428 Bryan, S. P., Marchitto, T. M., & Lehman, S. J. (2010). The release of 14C-depleted carbon from the deep ocean  
429 during the last deglaciation: Evidence from the Arabian Sea. *Earth and Planetary Science Letters*, 298(1),  
430 244–254. <https://doi.org/10.1016/j.epsl.2010.08.025>
- 431 Cartapanis, O., Galbraith, E. D., Bianchi, D., & Jaccard, S. L. (2018). Carbon burial in deep-sea sediment and  
432 implications for oceanic inventories of carbon and alkalinity over the last glacial cycle. *Climate of the Past*,  
433 14(11), 1819–1850. <https://doi.org/10.5194/cp-14-1819-2018>

- 434 Chen, T., Robinson, L. F., Burke, A., Claxton, L., Hain, M. P., Li, T., Rae, J. W. B., Stewart, J., Knowles, T. D. J.,  
435 Fornari, D. J., & Harpp, K. S. (2020). Persistently well-ventilated intermediate-depth ocean through the last  
436 deglaciation. *Nature Geoscience*, *13*(11), Article 11. <https://doi.org/10.1038/s41561-020-0638-6>
- 437 De Pol-Holz, R., Keigwin, L., Southon, J., Hebbeln, D., & Mohtadi, M. (2010). No signature of abyssal carbon in  
438 intermediate waters off Chile during deglaciation. *Nature Geoscience*, *3*(3), Article 3.  
439 <https://doi.org/10.1038/ngeo745>
- 440 Dinauer, A., Adolphi, F., & Joos, F. (2020). Mysteriously high  $\Delta^{14}\text{C}$  of the glacial atmosphere: Influence of  $^{14}\text{C}$   
441 production and carbon cycle changes. *Climate of the Past*, *16*(4), 1159–1185. [https://doi.org/10.5194/cp-](https://doi.org/10.5194/cp-16-1159-2020)  
442 [16-1159-2020](https://doi.org/10.5194/cp-16-1159-2020)
- 443 Gehrie, E., Archer, D., Emerson, S., Stump, C., & Henning, C. (2006). Subsurface ocean argon disequilibrium  
444 reveals the equatorial Pacific shadow zone. *Geophysical Research Letters*, *33*(18).  
445 <https://doi.org/10.1029/2006GL026935>
- 446 Hain, M. P., Sigman, D. M., & Haug, G. H. (2010). Carbon dioxide effects of Antarctic stratification, North Atlantic  
447 Intermediate Water formation, and subantarctic nutrient drawdown during the last ice age: Diagnosis and  
448 synthesis in a geochemical box model. *Global Biogeochemical Cycles*, *24*(4), n/a-n/a.  
449 <https://doi.org/10.1029/2010GB003790>
- 450 Hain, M. P., Sigman, D. M., & Haug, G. H. (2011). Shortcomings of the isolated abyssal reservoir model for  
451 deglacial radiocarbon changes in the mid-depth Indo-Pacific Ocean. *Geophysical Research Letters*, *38*(4).  
452 <https://doi.org/10.1029/2010GL046158>
- 453 Hain, M. P., Sigman, D. M., & Haug, G. H. (2014). Distinct roles of the Southern Ocean and North Atlantic in the  
454 deglacial atmospheric radiocarbon decline. *Earth and Planetary Science Letters*, *394*, 198–208.  
455 <https://doi.org/10.1016/j.epsl.2014.03.020>
- 456 Hodell, D. A., Venz, K. A., Charles, C. D., & Ninnemann, U. S. (2003). Pleistocene vertical carbon isotope and  
457 carbonate gradients in the South Atlantic sector of the Southern Ocean. *Geochemistry, Geophysics,*  
458 *Geosystems*, *4*(1), 1–19. <https://doi.org/10.1029/2002GC000367>
- 459 Holzer, M., DeVries, T., & de Lavergne, C. (2021). Diffusion controls the ventilation of a Pacific Shadow Zone  
460 above abyssal overturning. *Nature Communications*, *12*(1), Article 1. [https://doi.org/10.1038/s41467-021-](https://doi.org/10.1038/s41467-021-24648-x)  
461 [24648-x](https://doi.org/10.1038/s41467-021-24648-x)

- 462 Huybers, P., & Langmuir, C. (2009). Feedback between deglaciation, volcanism, and atmospheric CO<sub>2</sub>. *Earth and*  
463 *Planetary Science Letters*, 286(3), 479–491. <https://doi.org/10.1016/j.epsl.2009.07.014>
- 464 Ito, T., & Follows, M. J. (2005). Preformed phosphate, soft tissue pump and atmospheric CO<sub>2</sub>. *Journal of Marine*  
465 *Research*, 63(4), 813–839. <https://doi.org/10.1357/0022240054663231>
- 466 Joos, F., Prentice, I. C., Sitch, S., Meyer, R., Hooss, G., Plattner, G.-K., Gerber, S., & Hasselmann, K. (2001).  
467 Global warming feedbacks on terrestrial carbon uptake under the Intergovernmental Panel on Climate  
468 Change (IPCC) Emission Scenarios. *Global Biogeochemical Cycles*, 15(4), 891–907.  
469 <https://doi.org/10.1029/2000GB001375>
- 470 Keir, R. S. (1988). On the Late Pleistocene ocean geochemistry and circulation. *Paleoceanography*, 3(4), 413–445.  
471 <https://doi.org/10.1029/PA003i004p00413>
- 472 Khatiwala, S., Schmittner, A., & Muglia, J. (2019). Air-sea disequilibrium enhances ocean carbon storage during  
473 glacial periods. *Science Advances*, 5(6), eaaw4981. <https://doi.org/10.1126/sciadv.aaw4981>
- 474 Köhler, P., Knorr, G., & Bard, E. (2014). Permafrost thawing as a possible source of abrupt carbon release at the  
475 onset of the Bølling/Allerød. *Nature Communications*, 5(1), Article 1. <https://doi.org/10.1038/ncomms6520>
- 476 Lindsay, C. M., Lehman, S. J., Marchitto, T. M., Carriquiry, J. D., & Ortiz, J. D. (2016). New constraints on  
477 deglacial marine radiocarbon anomalies from a depth transect near Baja California. *Paleoceanography*,  
478 31(8), 1103–1116. <https://doi.org/10.1002/2015PA002878>
- 479 Lindsay, C. M., Lehman, S. J., Marchitto, T. M., & Ortiz, J. D. (2015). The surface expression of radiocarbon  
480 anomalies near Baja California during deglaciation. *Earth and Planetary Science Letters*, 422, 67–74.  
481 <https://doi.org/10.1016/j.epsl.2015.04.012>
- 482 Marchitto, T. M., Lehman, S. J., Ortiz, J. D., Fluckiger, J., & van Geen, A. (2007). Marine Radiocarbon Evidence  
483 for the Mechanism of Deglacial Atmospheric CO<sub>2</sub> Rise. *Science*, 316(5830), 1456–1459.  
484 <https://doi.org/10.1126/science.1138679>
- 485 Marcott, S. A., Bauska, T. K., Buizert, C., Steig, E. J., Rosen, J. L., Cuffey, K. M., Fudge, T. J., Severinghaus, J. P.,  
486 Ahn, J., Kalk, M. L., McConnell, J. R., Sowers, T., Taylor, K. C., White, J. W. C., & Brook, E. J. (2014).  
487 Centennial-scale changes in the global carbon cycle during the last deglaciation. *Nature*, 514(7524), Article  
488 7524. <https://doi.org/10.1038/nature13799>

- 489 Margolskee, A., Frenzel, H., Emerson, S., & Deutsch, C. (2019). Ventilation Pathways for the North Pacific Oxygen  
490 Deficient Zone. *Global Biogeochemical Cycles*, 33(7), 875–890. <https://doi.org/10.1029/2018GB006149>
- 491 Marinov, I., Follows, M., Gnanadesikan, A., Sarmiento, J. L., & Slater, R. D. (2008). How does ocean biology affect  
492 atmospheric pCO<sub>2</sub>? Theory and models. *Journal of Geophysical Research: Oceans*, 113(C7).  
493 <https://doi.org/10.1029/2007JC004598>
- 494 Marinov, I., Gnanadesikan, A., Sarmiento, J. L., Toggweiler, J. R., Follows, M., & Mignone, B. K. (2008). Impact  
495 of oceanic circulation on biological carbon storage in the ocean and atmospheric pCO<sub>2</sub>. *Global  
496 Biogeochemical Cycles*, 22(3). <https://doi.org/10.1029/2007GB002958>
- 497 McManus, J. F., Francois, R., Gherardi, J.-M., Keigwin, L. D., & Brown-Leger, S. (2004). Collapse and rapid  
498 resumption of Atlantic meridional circulation linked to deglacial climate changes. *Nature*, 428(6985),  
499 Article 6985. <https://doi.org/10.1038/nature02494>
- 500 NASEM. (2022). *A Research Strategy for Ocean-based Carbon Dioxide Removal and Sequestration*. The National  
501 Academies Press. <https://doi.org/10.17226/26278>
- 502 Ortiz, J. D., O’Connell, S. B., DelViscio, J., Dean, W., Carriquiry, J. D., Marchitto, T., Zheng, Y., & Van Geen, A.  
503 (2004). Enhanced marine productivity off western North America during warm climate intervals of the past  
504 52 k.y. *Geology*, 32(6), 521. <https://doi.org/10.1130/G20234.1>
- 505 Poggemann, D.-W., Nürnberg, D., Hathorne, E. C., Frank, M., Rath, W., Reißig, S., & Bahr, A. (2018). Deglacial  
506 Heat Uptake by the Southern Ocean and Rapid Northward Redistribution Via Antarctic Intermediate  
507 Water. *Paleoceanography and Paleoclimatology*, 33(11), 1292–1305.  
508 <https://doi.org/10.1029/2017PA003284>
- 509 Pollack, H. N., Hurter, S. J., & Johnson, J. R. (1993). Heat flow from the Earth’s interior: Analysis of the global data  
510 set. *Reviews of Geophysics*, 31(3), 267–280. <https://doi.org/10.1029/93RG01249>
- 511 Rafter, P. A., Carriquiry, J. D., Herguera, J., Hain, M. P., Solomon, E. A., & Southon, J. R. (2019). Anomalous >  
512 2000-Year-Old Surface Ocean Radiocarbon Age as Evidence for Deglacial Geologic Carbon Release.  
513 *Geophysical Research Letters*, 46(23), 13950–13960. <https://doi.org/10.1029/2019GL085102>
- 514 Rafter, P. A., Gray, W. R., Hines, S. K. V., Burke, A., Costa, K. M., Gottschalk, J., Hain, M. P., Rae, J. W. B.,  
515 Southon, J. R., Walczak, M. H., Yu, J., Adkins, J. F., & DeVries, T. (2022). Global reorganization of deep-

- 516 sea circulation and carbon storage after the last ice age. *Science Advances*, 8(46), eabq5434.  
517 <https://doi.org/10.1126/sciadv.abq5434>
- 518 Rafter, P. A., Herguera, J.-C., & Southon, J. R. (2018). Extreme lowering of deglacial seawater radiocarbon  
519 recorded by both epifaunal and infaunal benthic foraminifera in a wood-dated sediment core. *Climate of the  
520 Past*, 14(12), 1977–1989. <https://doi.org/10.5194/cp-14-1977-2018>
- 521 Reimer, P. J., Austin, W. E. N., Bard, E., Bayliss, A., Blackwell, P. G., Ramsey, C. B., Butzin, M., Cheng, H.,  
522 Edwards, R. L., Friedrich, M., Grootes, P. M., Guilderson, T. P., Hajdas, I., Heaton, T. J., Hogg, A. G.,  
523 Hughen, K. A., Kromer, B., Manning, S. W., Muscheler, R., ... Talamo, S. (2020). The IntCal20 Northern  
524 Hemisphere Radiocarbon Age Calibration Curve (0–55 cal kBP). *Radiocarbon*, 62(4), 725–757.  
525 <https://doi.org/10.1017/RDC.2020.41>
- 526 Ronge, T. A., Tiedemann, R., Lamy, F., Köhler, P., Alloway, B. V., De Pol-Holz, R., Pahnke, K., Southon, J., &  
527 Wacker, L. (2016). Radiocarbon constraints on the extent and evolution of the South Pacific glacial carbon  
528 pool. *Nature Communications*, 7(1), 11487. <https://doi.org/10.1038/ncomms11487>
- 529 Rose, K. A., Sikes, E. L., Guilderson, T. P., Shane, P., Hill, T. M., Zahn, R., & Spero, H. J. (2010). Upper-ocean-to-  
530 atmosphere radiocarbon offsets imply fast deglacial carbon dioxide release. *Nature*, 466(7310), Article  
531 7310. <https://doi.org/10.1038/nature09288>
- 532 Roth, R., & Joos, F. (2012). Model limits on the role of volcanic carbon emissions in regulating glacial–interglacial  
533 CO<sub>2</sub> variations. *Earth and Planetary Science Letters*, 329–330, 141–149.  
534 <https://doi.org/10.1016/j.epsl.2012.02.019>
- 535 Roth, R., & Joos, F. (2013). A reconstruction of radiocarbon production and total solar irradiance from the Holocene  
536 <sup>14</sup>C and CO<sub>2</sub> records: Implications of data and model uncertainties. *Climate of the Past*, 9(4), 1879–1909.  
537 <https://doi.org/10.5194/cp-9-1879-2013>
- 538 Shakun, J. D., Clark, P. U., He, F., Marcott, S. A., Mix, A. C., Liu, Z., Otto-Bliesner, B., Schmittner, A., & Bard, E.  
539 (2012). Global warming preceded by increasing carbon dioxide concentrations during the last deglaciation.  
540 *Nature*, 484(7392), Article 7392. <https://doi.org/10.1038/nature10915>
- 541 Siani, G., Michel, E., De Pol-Holz, R., DeVries, T., Lamy, F., Carel, M., Isguder, G., Dewilde, F., & Laurantou, A.  
542 (2013). Carbon isotope records reveal precise timing of enhanced Southern Ocean upwelling during the last  
543 deglaciation. *Nature Communications*, 4(1), Article 1. <https://doi.org/10.1038/ncomms3758>

- 544 Siegenthaler, U., Stocker, T. F., Monnin, E., Lüthi, D., Schwander, J., Stauffer, B., Raynaud, D., Barnola, J.-M.,  
545 Fischer, H., Masson-Delmotte, V., & Jouzel, J. (2005). Stable Carbon Cycle–Climate Relationship During  
546 the Late Pleistocene. *Science*, *310*(5752), 1313–1317. <https://doi.org/10.1126/science.1120130>
- 547 Sigman, D. M., Fripiat, F., Studer, A. S., Kemeny, P. C., Martínez-García, A., Hain, M. P., Ai, X., Wang, X., Ren,  
548 H., & Haug, G. H. (2020). The Southern Ocean during the ice ages: A review of the Antarctic surface  
549 isolation hypothesis, with comparison to the North Pacific. *Quaternary Science Reviews*, 106732.  
550 <https://doi.org/10.1016/j.quascirev.2020.106732>
- 551 Sigman, D. M., Fripiat, F., Studer, A. S., Kemeny, P. C., Martínez-García, A., Hain, M. P., Ai, X., Wang, X., Ren,  
552 H., & Haug, G. H. (2021). The Southern Ocean during the ice ages: A review of the Antarctic surface  
553 isolation hypothesis, with comparison to the North Pacific. *Quaternary Science Reviews*, *254*, 106732.  
554 <https://doi.org/10.1016/j.quascirev.2020.106732>
- 555 Sigman, D. M., Hain, M. P., & Haug, G. H. (2010). The polar ocean and glacial cycles in atmospheric CO<sub>2</sub>  
556 concentration. *Nature*, *466*(7302), 47–55. <https://doi.org/10.1038/nature09149>
- 557 Sigman, D. M., & Haug, G. H. (2003). *6.18 The Biological Pump in the Past*.
- 558 Skinner, L. C., & Bard, E. (2022). Radiocarbon as a Dating Tool and Tracer in Paleoceanography. *Reviews of*  
559 *Geophysics*, *60*(1), e2020RG000720. <https://doi.org/10.1029/2020RG000720>
- 560 Skinner, L. C., Fallon, S., Waelbroeck, C., Michel, E., & Barker, S. (2010). Ventilation of the Deep Southern Ocean  
561 and Deglacial CO<sub>2</sub> Rise. *Science*, *328*(5982), 1147–1151. <https://doi.org/10.1126/science.1183627>
- 562 Stott, L. D., Harazin, K. M., & Krupinski, N. B. Q. (2019). Hydrothermal carbon release to the ocean and  
563 atmosphere from the eastern equatorial Pacific during the last glacial termination. *Environmental Research*  
564 *Letters*, *14*(2), 025007. <https://doi.org/10.1088/1748-9326/aafe28>
- 565 Stott, L., Southon, J., Timmermann, A., & Koutavas, A. (2009). Radiocarbon age anomaly at intermediate water  
566 depth in the Pacific Ocean during the last deglaciation. *Paleoceanography*, *24*(2), n/a-n/a.  
567 <https://doi.org/10.1029/2008PA001690>
- 568 Stott, L., & Timmermann, A. (2011). Hypothesized Link Between Glacial/Interglacial Atmospheric CO<sub>2</sub> Cycles and  
569 Storage/Release of CO<sub>2</sub>-Rich Fluids From Deep-Sea Sediments. In H. Rashid, L. Polyak, & E. Mosley-  
570 Thompson (Eds.), *Geophysical Monograph Series* (Vol. 193, pp. 123–138). American Geophysical Union.  
571 <https://doi.org/10.1029/2010GM001052>

- 572 Stuiver, M., & Polach, H. A. (1977). Discussion Reporting of  $^{14}\text{C}$  Data. *Radiocarbon*, 19(3), 355–363.  
573 <https://doi.org/10.1017/S0033822200003672>
- 574 Yu, J., Anderson, R. F., Jin, Z., Rae, J. W. B., Opdyke, B. N., & Eggins, S. M. (2013). Responses of the deep ocean  
575 carbonate system to carbon reorganization during the Last Glacial–interglacial cycle. *Quaternary Science*  
576 *Reviews*, 76, 39–52. <https://doi.org/10.1016/j.quascirev.2013.06.020>
- 577 Yu, J., Broecker, W. S., Elderfield, H., Jin, Z., McManus, J., & Zhang, F. (2010). Loss of Carbon from the Deep Sea  
578 Since the Last Glacial Maximum. *Science*, 330(6007), 1084–1087. <https://doi.org/10.1126/science.1193221>
- 579 Yu, J., Elderfield, H., & Piotrowski, A. M. (2008). Seawater carbonate ion- $\delta^{13}\text{C}$  systematics and application to  
580 glacial–interglacial North Atlantic ocean circulation. *Earth and Planetary Science Letters*, 271(1), 209–  
581 220. <https://doi.org/10.1016/j.epsl.2008.04.010>
- 582 Zhao, N., & Keigwin, L. D. (2018). An atmospheric chronology for the glacial-deglacial Eastern Equatorial Pacific.  
583 *Nature Communications*, 9(1), Article 1. <https://doi.org/10.1038/s41467-018-05574-x>
- 584